

PAPER

View Article Online
View Journal | View IssueCite this: *J. Mater. Chem. A*, 2018, 6,
21193Synthesis of glycopolymer nanosponges with
enhanced adsorption performances for boron
removal and water treatment†Xueping Liao,^{ab} Bingyu Wang^{ab} and Qiang Zhang  ^{*ab}

The high-affinity interactions between *cis*-diols and boric/boronic acid have been widely employed as a tool for carbohydrate analysis, protein separation and boron removal. Herein we report the design and synthesis of cyclodextrin-scaffolded glycopolymers as bifunctional nanosponges for boron removal and water treatment for the first time. Different glycopolymer nanosponges (GNs) have been successfully synthesized from monosaccharides and β -cyclodextrin via a combination of a cross-linking reaction, Fischer glycosylation and a click reaction. Such functional GNs are mesoporous polymer frameworks with *cis*-diol-containing saccharides immobilized on the surface, which have exhibited selective adsorption behaviour towards boric acid depending on the structure of the GNs and the loaded saccharides. The GNs have also shown remarkable adsorption rates and capacities for an organic dye as a model pollutant in this work. Secondary bonding, such as hydrogen bonding and van der Waals forces between the immobilized saccharides and the adsorbates is believed to be responsible for the significantly enhanced adsorption rates and capacities. Such bifunctional materials may exhibit potential applications in seawater desalination and water treatment.

Received 14th July 2018
Accepted 8th October 2018

DOI: 10.1039/c8ta06802j

rsc.li/materials-a

Introduction

Water scarcity has become one of the most serious challenges facing the world today and there is great potential to address the worldwide water-shortage problem by converting nearly inexhaustible seawater into fresh water using desalination technologies.^{1–3} Although most salts could be removed by reverse osmosis (RO) desalination technology, it is still a challenge to remove boron. This is mainly due to the existence of boron as neutrally charged boric acid in seawater and its ability to efficiently diffuse through RO membranes like water molecules, which will result in unsatisfactory levels of residual boron in the permeate water.^{4,5} Since the discovery by Hermans, Böeseken *et al.* that *cis*-diol-containing molecules could coordinate with boric acid to form stable borate esters, polyols have been extensively applied for the removal of boron from water.^{6,7} Functional polyols such as *N*-methylglucamine, imino-bispropane diol and phenol hydroxyl groups have been immobilized on the surface of ion exchange resins, membranes or

hybrid nanomaterials for selective removal of boron.^{8–11} Natural carbohydrate polymers (cellulose fibres *etc.*) and artificial polymeric nanomaterials have been used to achieve great success in water treatment and engineering, such as the efficient adsorption of heavy metal ions and organic dyes.^{12–17} Synthetic glycopolymers could reversibly complex with boronic acids by forming 5- or 6-membered ring cyclic borate esters, which is useful for the construction of glucose biosensors and smart materials.^{18–20} Compared with the chelating diol groups of pyranoses, borates have shown much higher affinity towards furanoses and form very stable boron esters with *D*-ribose.^{21,22} Most reports in the literature have focused on the study of interactions between pyranose-containing glycopolymers and phenylboronic acids (PBA) rather than boric acids, however, boron in nature mainly exist in the form of boric acid or boronate salts rather than PBA.²³ It is worth noting that even a slight excess of boric acid was reported to have toxic effects on the growth of some boron-sensitive agricultural crops.^{24,25} Thus it is imperative to develop an effective treatment technology for the removal of boric acid in order to match the specific restrictions of drinking and irrigation. To the best of our knowledge, few relevant studies on the synthesis of furanose-containing glycopolymers for bonding with boric acids have been performed thus far.

Activated carbons are the most widespread adsorbents for water purification; however, some deficiencies such as the slow uptake rate and poor removal of hydrophilic pollutants make them have poor performances in removing emerging organic

^aJiangsu Key Laboratory of Chemical Pollution Control and Resources Reuse, School of Environmental and Biological Engineering, Nanjing University of Science and Technology, Nanjing 210094, P. R. China

^bInstitute of Polymer Ecomaterials, School of Environmental and Biological Engineering, Nanjing University of Science and Technology, Nanjing 210094, P. R. China. E-mail: zhangqiang@njust.edu.cn

† Electronic supplementary information (ESI) available. See DOI: 10.1039/c8ta06802j

micropollutants from water.²⁶ Cyclodextrins (CDs) are well-known supermolecules with hydrophobic interior cavities, which could encapsulate thousands of different organic pollutants *via* host-guest interactions and thus become potential candidates for adsorption and separation. Chemical cross-linking of CDs with bifunctional crosslinking agents in alkaline media resulted in the formation of polymeric networks, which have already shown extraordinary abilities in the selective removal of heavy metal ions or cationic dyes from aqueous solutions.^{27–29} Studies using tetrafluoroterephthalonitrile or decafluorobiphenyl *etc.* as novel crosslinking agents have raised great attention recently, which is mainly attributed to the abilities of the generated highly porous CD polymers with ultrafast adsorption rates of organic micropollutants from water.^{26,30–32} However, most hydroxyl groups in the CD polymers are either substituted, coordinated or not in a *cis* configuration, thus no boron adsorption ability could be attained.

Position- and face-selective modifications of CDs with functional saccharides, which were mainly through click-type ligation chemistry, have generated a wide family of CD-scaffolded glycoclusters over the past few decades.^{33–36} These glycoclusters have been well developed, especially in the research of optimizing carbohydrate-protein interactions, drug delivery and anti-adhesion therapy.^{37–40} Recently mannose or glucose functionalized CD glycoclusters have been used for the construction of molecular recognition surfaces *via* host-guest interactions.^{41–45} Specific capture and release of proteins and bacteria could be realized due to the presence of a multivalency effect between the glycoclusters and the biomacromolecules.^{42,43,45} The dynamic covalent bonding between PBA and secondary hydroxyls of CD-functionalized supermolecules was proven to be sugar-responsive, however, this system has not been applied to the adsorption of boric acid due to the specific preference for *cis*-diols.⁴⁶ Due to the combination of hydrophobic interior cavities and functional saccharides, it could be reasonable to hypothesize that such CD-scaffolded glycoclusters could act as potential candidates for the simultaneous encapsulation of organic pollutants and adsorption of boron. However, these glycoclusters are generally highly water-soluble due to the presence of saccharides and it is hard to remove them from aqueous solution after water treatment. We believe that cross-linked CD polymers with persubstituted multivalent saccharides could theoretically combine hydrophobic cavities and glycoligand arrays together, while the insoluble polymer networks could endow the materials with good recyclability.

This study herein develops the synthesis of CD-scaffolded glycopolymers and investigates the possibility of using such glycopolymers as bifunctional nanosponges to remove boron and organic pollutants from aqueous solution. To the best of our knowledge, this is the first report of CD glycopolymers with the ability to adsorb boric acids. A facile synthetic route *via* the combination of a cross-linking reaction, Fischer glycosylation and a copper-mediated azide-alkyne cycloaddition reaction (CuAAC) was developed for the construction of varied GNs with controlled CD compositions and various functional saccharides. The properties of such GNs for the adsorption of boron and organic pollutants were also evaluated respectively.

Experimental

Materials

β -Cyclodextrin (β -CD, 96%, Aladdin, China) was recrystallized twice from water in order to improve the purity and dried in a vacuum oven at 100 °C for two days before use. Heptakis(6-deoxy-6-azido)- β -cyclodextrin (β -CD-(N₃)₇) and H₂SO₄-silica catalyst were synthesized according to previous reports.^{40,47–49} 1-(2'-Propargyl)-D-glucose, 1-(2'-propargyl)-D-mannose, 1-(2'-propargyl)-N-acetyl-D-glucosamine and 1-(2'-propargyl)-D-ribose were prepared according to procedures described in previous literature.^{48,49} D-(+)-Gluconic acid δ -lactone (99%), propargylamine (98%), terephthaloyl chloride (TCL, 99%), copper(II) sulfate pentahydrate (CuSO₄·5H₂O, 99%), (+)-sodium L-ascorbate (NaAsc, 98%), boric acid (99.5%) and methylene blue (MB, dye content \geq 90% (HPLC)) were obtained from Aladdin (China) and used directly. All the other reagents and anhydrous solvents were obtained at analytical grade (>99%) from Aladdin (China) and used without further purification unless otherwise stated.

Characterization techniques

¹H and ¹³C NMR spectra were recorded on a Bruker Avance 500 MHz spectrometer using deuterated solvents obtained from Aladdin. The NMR spectrometer had a BBFO-Plus forward broadband liquid probe. The probe temperature was 25 °C during the test, the number of ¹H scans was 16, and the number of ¹³C scans was 300. Fourier Transform Infrared Spectroscopy (FTIR) measurements were carried out using a Nicolet iS5 FTIR spectrometer using an iD7 diamond attenuated total reflectance optical base and thirty-two scans were taken for each spectrum at a normal resolution of 2 cm⁻¹. Mass spectrometric data was measured using a Bruker Daltonics APE III ESI spectrometer. Surface area and pore structure parameters of the adsorbents were measured from N₂ adsorption/desorption isotherms at -196 °C (77 K) using a TriStar II 3020 V1.03 system (Micromeritics Instrument Co., Norcross, GA, USA). Prior to N₂ adsorption, each sample (25–50 mg) was degassed at 90 °C under vacuum for 24 h and then backfilled with N₂. A UV/Vis spectrophotometer (SHIMADZU UV-2600) was utilized to measure the concentration of sample during adsorption at defined wavelengths. Elemental analysis (EA) was performed using an Elementar Vario MICRO. Thermal gravimetric analysis (TGA, Mettler Toledo, Switzerland) was performed at a heating rate of 10 °C min⁻¹ from room temperature to 800 °C under N₂ protection. Differential scanning calorimetry (DSC 823e, Mettler Toledo, Switzerland) was performed at a heating rate of 10 °C min⁻¹ from room temperature to 550 °C under N₂ protection (note: azide-containing compounds should be handled with care and the amount for TGA/DSC analysis was limited below 5 mg). Scanning electron microscope (SEM) images were taken using a field emission SEM (FEI Quant 250FEG, USA) after the synthesised cross-linked CD polymer samples were coated with a 20 nm gold layer.

Synthesis of cross-linked CD polymers

For the synthesis of the CD copolymer, β -CD (2.00 g, 1.76 mmol), (β -CD-(N₃)₇) (2.00 g, 1.53 mmol) and 50 mL anhydrous

pyridine were added to a flame dried three-neck round bottom-flask and stirred for 1 h to afford a homogeneous solution before being cooled to 0 °C *via* an ice/water bath. TCL (9.35 g, 46.06 mmol) dissolved in 20 mL anhydrous THF was then added dropwise to the pyridine solution. Subsequently, the reaction mixture was stirred at 70 °C for 4 h. After cooling down, 100 mL water was slowly added into the suspension and the resulting precipitates were filtered off and washed with excess water and acetone repeatedly. The final product, poly(β -CD)-*co*-(β -CD-(N₃)₇), was obtained as a white solid (9.69 g) after drying under vacuum at 100 °C for one day.

For the synthesis of the CD homopolymers, only β -CD-(N₃)₇ (2.00 g, 1.53 mmol) or β -CD (2.17 g, 1.91 mmol) was used and the reaction was performed *via* the same procedure with only decreased amounts of TCL (4.34 g, 21.37 mmol for β -CD-(N₃)₇; 5.43 g, 26.78 mmol for β -CD) and solvents (pyridine, 30 mL; THF, 10 mL). The poly(β -CD-(N₃)₇) and poly(β -CD) were obtained as white solids after drying under vacuum at 100 °C for one day.

Synthesis of *N*-(prop-2-yn-1-yl) β -gluconamide

In a 250 mL round-bottom flask equipped with a magnetic stirrer bar, *D*-(+)-gluconic acid δ -lactone (10 g, 56.2 mmol) and propargylamine (5.32 g, 96.6 mmol) were dissolved in methanol (100 mL). The solution was stirred under ambient temperature and after 0.5 h a flocculent precipitate started to appear in the flask. The amount of precipitate stopped increasing after ~5 h and thus the reaction was stopped. The suspension was concentrated *via* rotary evaporation to a quarter of its original volume and then poured into an excess of DCM. The formed white precipitate was filtered off and washed with DCM and 2-propanol alcohol repeatedly. The final product, (2*R*,3*R*,4*R*,5*S*)-2,3,4,5,6-pentahydroxy-*N*-(prop-2-yn-1-yl)hexanamide (*N*-(prop-2-yn-1-yl) β -gluconamide) was obtained as white crystals after drying under vacuum (5.89 g, yield: 45%).

¹H NMR (D₂O, 500 MHz, 298 K): δ 4.32 (d, *J* = 3.81 Hz, 1H, C=O-C-H), 3.60–4.15 (multiple peaks, sugar residues), 2.59 (t, *J* = 2.50 Hz, 1H, C=C-H) ppm. ¹³C NMR (D₂O, 125 MHz, 298 K): δ 173.5 (C=O), 78.5 (HC=C-CH₂), 72.3 (HC=C-CH₂), 71.0 (C=O-CH-), 70.8 (CH-CH₂-OH), 70.1 (C=O-CH-CH-), 69.5 (CH-CH-CH₂-OH), 61.7 (-CH₂-OH), 27.5 (HC=C-CH₂) ppm. FTIR *v*: 3498, 3325 (C=C-H), 3250, 2117 (C≡C), 1656 (C=O), 1525, 1039 cm⁻¹. ESI-MS *m/z* calcd for C₉H₁₅NO₆H⁺ (M + H) 234.09, found 234.07.

Synthesis of CD-scaffolded GNs *via* click chemistry

The typical reaction procedure was carried out as below. To a vial with a magnetic stirrer bar, poly(β -CD)-*co*-(β -CD-(N₃)₇) (500 mg), 1-(2'-propargyl) β -ribose (376 mg, 2 mmol), CuSO₄·5H₂O (37 mg, 0.15 mmol) and water (5 mL) were added and the suspension was degassed *via* nitrogen bubbling for 10 min. Subsequently, 1 mL of a degassed aqueous solution containing NaAsc (44 mg, 0.22 mmol) was added into the suspension and reacted at 50 °C for one day. After the reaction, the solution was removed *via* centrifugation and the solids were re-dispersed in water by ultra-sonication. The centrifugation-wash cycle was

repeated at least six times in order to remove any unreacted monosaccharides or residual catalyst. The cross-linked CD-scaffolded glycocluster, poly(β -CD)-*co*-(β -CD-(N₃)₇)@ribose, was obtained as a white powder after lyophilization.

Adsorption and regeneration experiments

Briefly, each 50 mL vial with a polytetrafluoroethylene-lined screw cap received 100 mg or 10 mg of the GN samples and DI water as a background solution. The sorbent samples were pre-wetted for 12 h and a pre-determined volume of a sorbate stock solution (prepared in DI water) was added to achieve an initial concentration of 300 mg L⁻¹ for boron and 400 mg L⁻¹ for methylene blue (MB). The samples were covered with aluminium foil and shaken by an orbital shaker incubated at 25 °C and 100 rpm for 24 h. This duration was sufficient to reach an apparent sorption equilibrium (no further uptake of sorbate) according to the adsorption kinetics data as discussed later. Afterwards, 1 mL of boron or 0.5 mL of MB was withdrawn from the vials, filtered through a 0.22 μ m MCE filter head to remove the sorbents, and analyzed by UV-vis spectrometry (see below). The filter membrane was proved to have a negligible sorption amount after filtration of the adsorbates compared without filtration. To take into account any potential adsorbate loss to experimental apparatus (*e.g.*, glassware and septum) or through volatilization during the experiments, calibration curves were obtained from control treatments that underwent the same experimental procedure without any sorbent added. Calibration curves included at least 6 standard concentration levels to cover the test concentration range. The sorbed mass of adsorbate was calculated from the difference between the initial and final aqueous-phase masses, and was calculated using the following equation:

$$Q_e = \frac{(C_0 - C_t)V}{M} \quad (1)$$

where *C*₀ and *C*_{*t*} are the initial and final concentrations (mg L⁻¹), respectively. *M* (g) and *V* (L) represent the weight of the adsorbent and the volume of solution.

The MB adsorption data were fitted with two commonly used nonlinear adsorption models:

The Freundlich model,

$$Q_e = K_F C_e^n \quad (2)$$

where *K*_F (mg^{1-*n*} L^{*n*} g⁻¹) is the Freundlich affinity coefficient and *n* (unitless) is the Freundlich linearity index;

The Langmuir model,

$$Q_e = \frac{K_L C_e}{1 + K_L C_e} Q_{\max} \quad (3)$$

where *K*_L (L mg⁻¹) is the Langmuir affinity coefficient and *Q*_{max} (mg g⁻¹) is the maximum adsorption capacity.

Single batch experiments were conducted to assess the adsorption kinetics with repeated sampling (1 mL of boron or 0.5 mL of MB each time for analysis) using 100 mL vials. The initial concentration of boron was 300 mg L⁻¹ with a pH value of 9.2 and the initial concentration of MB was 400 mg L⁻¹ with

a pH value of 6.8. The kinetic data were subsequently described by pseudo-first-order and pseudo-second-order kinetics models,

$$\log(Q_e - Q_t) = \log(Q_e) - \frac{k_1 t}{2.303} \quad (4)$$

$$\frac{t}{Q_t} = \frac{1}{k_2 Q_e^2} + \frac{t}{Q_e} \quad (5)$$

To evaluate the reusability of the adsorbents for the adsorption of boric acid, regeneration was performed by acid leaching. The regenerated sample was rinsed in HCl solution (pH = 3) and shaken overnight, then neutralized with DI water, and dried *via* lyophilization for re-adsorption. The adsorbents, after adsorption of MB, were regenerated by efficient washing with solution. Firstly, the sample was immersed in MeOH containing 5% of 1 M HCl and was shaken overnight, then the sample was washed with plenty of DI water, and was finally dried under vacuum.

The boron concentration was determined by UV-vis spectrometry using the Azomethine-H acid method.⁵⁰ The MB concentration was analyzed by UV-vis spectrometry in full spectrum mode (185–800 nm) or single wavelength mode (610 nm). Unless otherwise stated, error bars in all figures represent standard deviations calculated from triplicates.

Results and discussion

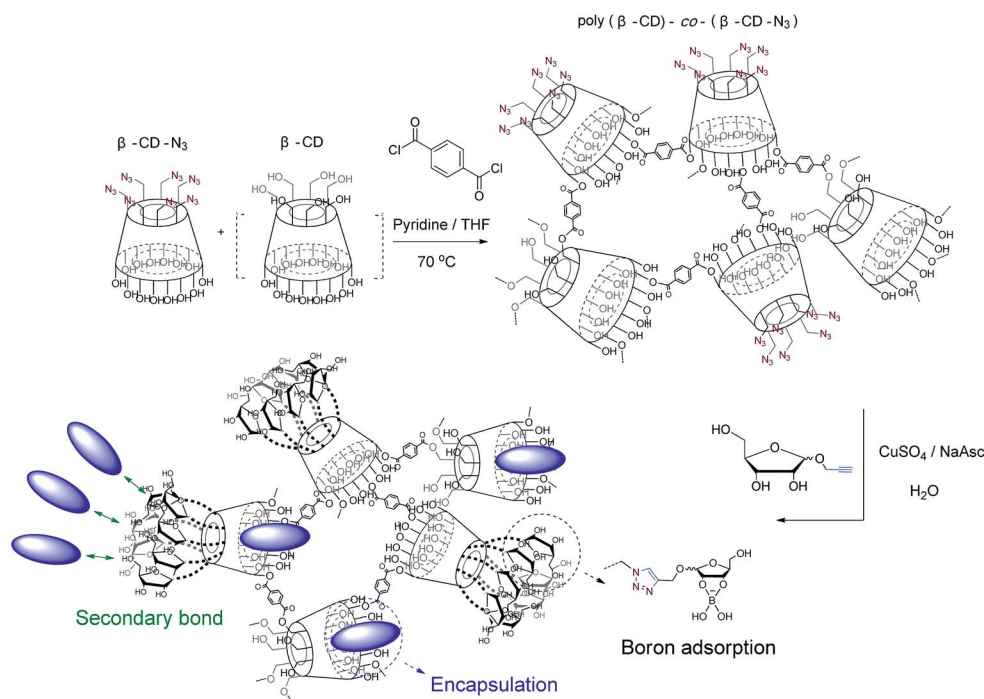
Synthesis and characterization of bifunctional GNs

The total synthesis route of the cross-linked GNs is shown in Scheme 1. Firstly, terephthaloyl chloride (TCL) was used for

the cross-linking reaction of β -CD-(N₃)₇ to form an insoluble polymer framework with a CD core moiety and persubstituted azide groups on the primary face of the β -CD. Unmodified β -CD was selectively incorporated into the reaction to manipulate the ratio of azide functionality and the spatial structure of the GNs. After that, the CuAAC reactions of the CD polymer with alkyne-functionalized polyols were performed in order to generate the desired functional glycoclusters. The immobilized multivalent saccharides with *cis*-diols were used for coordination with boron or interaction with adsorbates *via* secondary bonding *etc.*, while the hydrophobic CD core could encapsulate organic molecules through the typical host-guest interactions.

TCL-cross-linked β -CD-(N₃)₇ in the presence and absence of β -CD, named as poly(β -CD)-*co*-(β -CD-(N₃)₇) and poly(β -CD-(N₃)₇) separately, have been synthesized as the scaffolds for further immobilization with *cis*-diol-containing saccharides. As shown in Fig. 1, FTIR spectra revealed the expected characteristic bands for the functional groups of the CD polymers, such as the azide groups at ~ 2100 cm⁻¹, the residual hydroxyl groups at ~ 3300 cm⁻¹ and the important ester linkage (C=O) at 1718 cm⁻¹. It is worth noting that the intensity of the absorption band from the azide group of poly(β -CD)-*co*-(β -CD-(N₃)₇) is much weaker than that of the poly(β -CD-(N₃)₇), probably due to the incorporation of β -CD which unavoidably decreased the relative content of azide functional groups in the polymer.

Subsequent elemental analysis (EA, Table 1) revealed that the weight content of nitrogen for the poly(β -CD-(N₃)₇) was 8.14%, which was 2 times higher than that of the poly(β -CD)-*co*-(β -CD-(N₃)₇) (3.51%) and further proved the presence of unmodified β -CD in the poly(β -CD)-*co*-(β -CD-(N₃)₇).



Scheme 1 Schematic representation of the synthesis of bifunctional GNs.

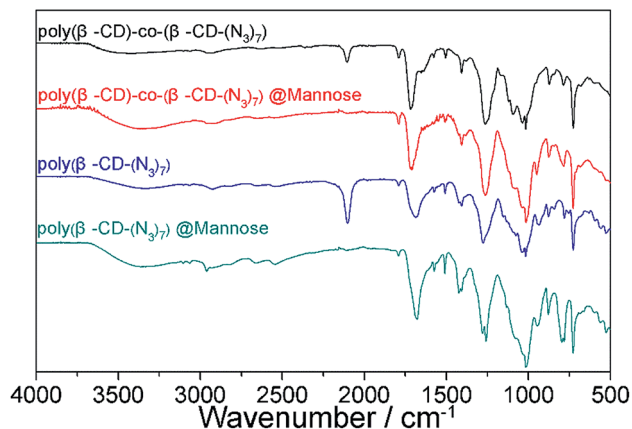


Fig. 1 FTIR spectra of the GNs obtained by click reaction.

Table 1 Elemental compositions for typical GNs

GNs	Elemental analysis (%)			
	C	H	N	O ^a
Poly(β-CD)-co-(β-CD-(N ₃) ₇)	54.87	4.11	3.55	37.47
Poly(β-CD)-co-(β-CD-(N ₃) ₇)@ribose	51.05	4.87	2.74	41.34
Poly(β-CD-(N ₃) ₇)	54.47	4.11	8.14	33.28
Poly(β-CD-(N ₃) ₇)@gluconolactone	47.67	4.75	7.43	40.15

^a Oxygen content calculated from measured C, H, and N values.

Thermogravimetric analyses (TGA, Fig. S1†) of poly(β-CD)-co-(β-CD-(N₃)₇) and poly(β-CD-(N₃)₇) both showed one sharp degradation step, centred at ~321 °C and 310 °C separately, which accounted for ~40% weight loss. Thus the incorporation of pristine β-CD will increase the thermal stability of the CD scaffold, possibly due to the higher crosslinking degree and the presence of less unstable β-CD-(N₃)₇ in the poly(β-CD)-co-(β-CD-(N₃)₇).

N₂ adsorption/desorption isotherms were then used for the characterization of the specific surface area (SSA) and pore parameters of the cross-linked CD polymers. As shown in Fig. 2, an obvious hysteresis loop in the range of $p/p_0 > 0.8$ and notably a sharp rise in the adsorbed volume for $p/p_0 > 0.9$ were observed in the N₂ adsorption/desorption isotherms. The SSA estimated for the poly(β-CD-(N₃)₇) was 21.02 m² g⁻¹, which is at the same level as those of typical urethane-based CD polymers.⁵¹ This value is relatively smaller than those of the activated carbons and certain porous β-CD-containing polymers such as the ones cross-linked by tetrafluoroterephthalonitrile *etc.*, however, it is larger than the SSA of CD-calixarene nanosponges with triazole linkers.^{26,52,53} Due to their limited N₂ adsorption, such polymers were considered as non-porous materials in previous reports; however, the SSA is much larger than that of the crystalline β-CD (0.635 m² g⁻¹ as previously reported) and thus the interstitial framework mesopores should not be overlooked.^{26,51} The average pore diameter calculated by the BJH adsorption isotherm was ~35 nm and the pore size distribution (Fig. 2, inset) suggests that the major contribution to the majority of

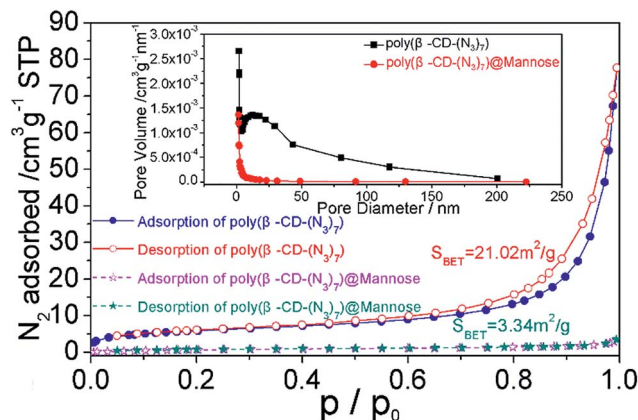
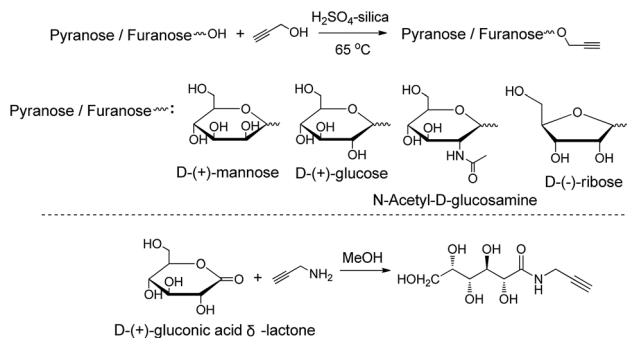


Fig. 2 N₂ adsorption (blue)/desorption (red) isotherms and pore volume vs. pore diameter (inset) for poly(β-CD-(N₃)₇) and poly(β-CD-(N₃)₇)@mannose. S_{BET} is the Brunauer–Emmett–Teller (BET) surface area (in units of m² g⁻¹) calculated from the N₂ adsorption isotherm; p and p_0 are the equilibrium and saturation pressures of N₂ at 77 K, respectively. The Barrett–Joyner–Halenda (BJH) method was used to estimate the pore volume and pore diameter from the adsorption isotherm.

the pore structure was from textural mesoporosity rather than the β-CD (~0.7–0.8 nm in diameter). All these results proved the successful synthesis of mesoporous polymers with a CD core moiety and azide functional groups.

Alkyne-functionalized polyols, including typical pyranoses, furanoses and chain-type polyol compounds, were then synthesized *via* a one-pot and one-step reaction as shown in Scheme 2. Different pyranoses and furanoses have been modified with alkyne groups *via* Fischer glycosylation for the synthesis of glycopolymers through a “post-polymerization modification” method.^{40,49,54,55} These glycosides were generally anomeric mixtures and were directly used without further separation. The mole ratio of an anomeric mixture (*e.g.* 1-(2'-propargyl)-D-ribose) could be defined by the adjacent triple peaks corresponding to the terminal alkynyl hydrogen at ~2.5 ppm in the ¹H NMR spectrum ($\alpha : \beta = 1 : 1$, Fig. S2†). The FTIR spectrum (Fig. S3†) also revealed the significant appearance of C–H and C≡C stretches of the terminal alkyne at ~3281 cm⁻¹ and ~2117 cm⁻¹ separately.

To expand the library of *cis*-diol-containing compounds rather than pyranose and furanose, an open-chain polyol



Scheme 2 Synthesis of alkyne-functionalized polyols.

compound was synthesized *via* the amidation reaction of D-(+)-gluconic acid δ -lactone with propargylamine. This mild reaction could give the target product without the need for chromatography purification. ^1H and ^{13}C NMR spectra were used to confirm the purity of the product and the numbering of the hydrogen and carbon atoms used for the NMR peak assignments is shown in Fig. 3. The FTIR spectra (Fig. S5†) also demonstrated the disappearance of absorbance from the ester bond ($\text{C}=\text{O}$) at $\sim 1750\text{ cm}^{-1}$ as well as the appearance of C–H and $\text{C}\equiv\text{C}$ stretches of the terminal alkyne at ~ 3325 and $\sim 2117\text{ cm}^{-1}$ and the amide bond ($\text{C}=\text{O}$) at $\sim 1650\text{ cm}^{-1}$. All of these reactions used inexpensive reagents and could be easily scaled up to 100 gram scale in the lab.

Subsequently, these *cis*-diol-containing compounds were immobilized to the CD polymers by CuAAC click reactions using $\text{CuSO}_4/\text{NaAsc}$ as the catalyst (Scheme 1). The successful synthesis of cross-linked glycoclusters could be proved by characterization using FTIR, EA, TGA and N_2 adsorption/desorption isotherms. As shown in Fig. 1 and S5,† the absorbance at $\sim 2100\text{ cm}^{-1}$ totally vanished, which indicated the complete consumption of the azide groups. The broad absorbance at $3000\text{--}3600\text{ cm}^{-1}$ increased dramatically due to the additional hydroxyl groups from the immobilized saccharides. For the products after the click reaction, the elemental compositions (Table 1) revealed a decrease in the nitrogen and carbon content accompanied with an increase of the hydrogen and oxygen content, which was mainly due to the higher content of hydrogen and oxygen in the immobilized saccharides. It is also worth noting that the nitrogen contents would theoretically decrease to 3.06% and 7.47% if the azide groups were totally reacted for $\text{poly}(\beta\text{-CD})\text{-co-(}\beta\text{-CD-(N}_3)_7\text{)}@$ ribose and $\text{poly}(\beta\text{-CD-(N}_3)_7)@$ gluconolactone respectively, which are very close to the experimental values (2.74% and 7.43% respectively). TGA analysis revealed a different thermal-decomposition behaviour after the click reaction. As shown in Fig. S1,† the GNs showed smoother traces after the click reaction compared with that of the TCL-cross-linked $\beta\text{-CD-(N}_3)_7$. After immobilization with more saccharides, the degradation of the GNs started at $\sim 120^\circ\text{C}$, which was much lower than that of the

$\text{poly}(\beta\text{-CD})\text{-co-(}\beta\text{-CD-(N}_3)_7\text{)}$ (up to $\sim 200^\circ\text{C}$, Fig. S1†). The differences in the thermal stabilities of the GNs are possibly owed to the varied chemical stabilities of the different saccharides. However, N_2 adsorption/desorption isotherms (Fig. 2) revealed a dramatic decrease of the SSA for $\text{poly}(\beta\text{-CD-(N}_3)_7)@$ mannose after the click reaction, from $21.02\text{ m}^2\text{ g}^{-1}$ to $3.34\text{ m}^2\text{ g}^{-1}$, which indicated that the addition of more saccharides may increase the packing density and attenuate the SSA of the framework. The pore size also significantly decreased to less than 5 nm (Fig. 2, inset) and revealed a change of pore structure. Interestingly, it was found that $\text{poly}(\beta\text{-CD})\text{-co-(}\beta\text{-CD-(N}_3)_7\text{)}@$ mannose showed a similar SSA as $\text{poly}(\beta\text{-CD})$ and $\text{poly}(\beta\text{-CD})\text{-co-(}\beta\text{-CD-(N}_3)_7\text{)}$ ranging from 15.2 to $22.5\text{ m}^2\text{ g}^{-1}$ (Fig. S6†). It was hypothesized that the existence of unmodified CD may reduce the occupation of the pore structure due to the click reaction.

Finally, the morphological properties of the GNs were investigated using scanning electron microscopy (SEM). As shown in Fig. 4, SEM images of $\text{poly}(\beta\text{-CD})\text{-co-(}\beta\text{-CD-(N}_3)_7\text{)}$ revealed the main presence of aggregated sphere-like nanoparticles with diameters ranging from $\sim 0.1\text{ }\mu\text{m}$ to $\sim 0.3\text{ }\mu\text{m}$. After the click reaction, the sphere-like morphology was retained for $\text{poly}(\beta\text{-CD})\text{-co-(}\beta\text{-CD-(N}_3)_7\text{)}@$ mannose; however, the surfaces of the spheres became rougher. Interestingly, aggregated irregular particles rather than spheres were found for the $\text{poly}(\beta\text{-CD-(N}_3)_7)$ and $\text{poly}(\beta\text{-CD-(N}_3)_7)@$ mannose. Pores and tunnels were found between these particles and may favour the efficient transport of small molecules into the GNs.

In summary, cross-linked GNs have been facilely synthesized from monosaccharides and $\beta\text{-CD}$ *via* a combination of a cross-linking reaction, glycosylation and click chemistry. These mesoporous polymer frameworks have multiple $\beta\text{-CD}$ cores as hydrophobic cavities and are covalently modified with different *cis*-diol-containing saccharides.

Boron removal performance of the varied functional GNs

Boron could be removed from water in the form of a borate ester, which was formed by the complexation reaction with

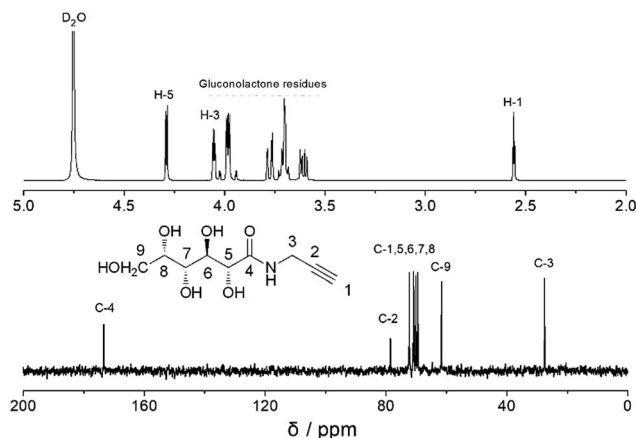


Fig. 3 ^1H and ^{13}C NMR spectra of *N*-(prop-2-yn-1-yl)-D-gluconamide in D_2O .

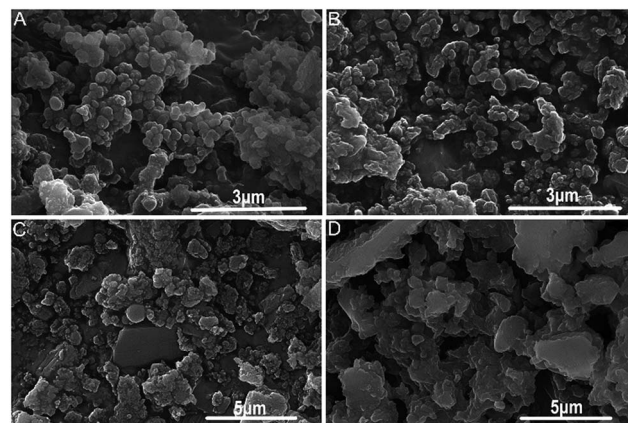


Fig. 4 SEM images of $\text{poly}(\beta\text{-CD})\text{-co-(}\beta\text{-CD-(N}_3)_7\text{)}$ (A), $\text{poly}(\beta\text{-CD})\text{-co-(}\beta\text{-CD-(N}_3)_7\text{)}@$ mannose (B), $\text{poly}(\beta\text{-CD-(N}_3)_7)$ (C) and $\text{poly}(\beta\text{-CD-(N}_3)_7)@$ mannose (D).

polyol groups immobilized on the surface of the adsorbents. Poly(β -CD)-*co*-(β -CD-(N₃)₇) and poly(β -CD-(N₃)₇) were first used for the boron adsorption and a commercially available boron-specific ion exchange resin (Amberlite IRA743) was used as a control test. The boron adsorption capacities of poly(β -CD)-*co*-(β -CD-(N₃)₇) and poly(β -CD-(N₃)₇) polymers were $-1.86 \pm 0.62 \text{ mg g}^{-1}$ and $-1.24 \pm 1.60 \text{ mg g}^{-1}$ respectively, which reveal that the unmodified CD polymers had almost no ability to adsorb boron, while under the same conditions, Amberlite resin showed a sorption capacity as high as $55.83 \pm 1.86 \text{ mg g}^{-1}$ (Table 2).

The presence of residual hydroxyl groups in the azide-functionalized CD polymers has been revealed clearly by the FTIR spectra (Fig. 1), however these hydroxyl groups of β -CD were either single hydroxyl groups or *trans*-diols and thus may not be able to coordinate with boron and form stable borate esters. Subsequently, different functional polyols were immobilized in order to supply *cis*-diols for complexation with boron. After poly(β -CD)-*co*-(β -CD-(N₃)₇) was covalently immobilized with mannose groups, the adsorption capacity tended to be very low ($0.87 \pm 1.67 \text{ mg g}^{-1}$). Although the hydroxyl groups from the carbons two, three, four and six are in adjacent positions, they orient in different directions and may not favour the formation of tetrahedrally coordinated structures. It has been reported that the 1, 2-diol or 1, 3-diol from glucose and *N*-acetyl-D-glucosamine could efficiently coordinate with phenylboronic acid or its derivatives to form stable phenylborates.^{20,56,57} For poly(β -CD)-*co*-(β -CD-(N₃)₇)@glucose and poly(β -CD)-*co*-(β -CD-(N₃)₇)@glucosamine, the adsorption capacities reached 4.45 ± 4.14 and $6.86 \pm 0.62 \text{ mg g}^{-1}$ (Table 2), respectively, which

suggested that the diols from these two saccharides could coordinate with borate more efficiently than the residual hydroxyls from CD. When these functional pyranoses were covalently linked to poly(β -CD-(N₃)₇), which theoretically contains more azide groups and thus more saccharides could be incorporated, the adsorption capacities of the obtained poly(β -CD-(N₃)₇)@mannose, poly(β -CD-(N₃)₇)@glucose and poly(β -CD-(N₃)₇)@glucosamine showed an unusual decreasing trend to almost zero, at 8.16 ± 2.74 , -2.78 ± 7.78 and $1.79 \pm 1.65 \text{ mg g}^{-1}$ (Table 1) respectively. This unusual decrease may be due to the significantly decreased SSA compared with the other GNs (Fig. 2), which may prevent the efficient contact of boron with the saccharides inside the GNs.

After that, a typical furanose, D-ribose, was covalently linked to the primary face of β -CD for boron adsorption. The adsorption capacity showed a significant increase to $19.04 \pm 4.39 \text{ mg g}^{-1}$ for poly(β -CD)-*co*-(β -CD-(N₃)₇)@ribose, which was much higher than the sorption capacity of the glucose or *N*-acetyl-D-glucosamine-functionalized glycoclusters. It has been reported that the local stability constants of the borate esters comprised of *cis*-1,2-diol furanose (2500–45 000) are hundreds or even several thousand times higher than those of the *cis*-1,2-diol pyranoses (10–20) and no coordination was observed when using *trans*-1,2-diol pyranoses/furanoses.^{22,58} Thus the coordination of the hydroxyl groups from carbons two and three of ribose with boron should be much more stable than that of the other pyranoses, which could explain the higher adsorption capacity. Interestingly, the poly(β -CD-(N₃)₇)@ribose containing more ribose also showed a low sorption capacity ($2.29 \pm 1.92 \text{ mg g}^{-1}$, Table 2) and accounted for only ~10% of the

Table 2 Boron adsorption capacity of the different GNs^a

Immobilized polyols (X) ^b	Structure	Sorption capacity (Q_e , mg g^{-1}) for	
		Poly(β -CD)- <i>co</i> -(β -CD-(N ₃) ₇)@X	Poly(β -CD-(N ₃) ₇)@X
β -CD residual		-1.86 ± 0.62	-1.24 ± 1.60
Mannose		0.87 ± 1.67	8.16 ± 2.74
Glucose		4.45 ± 4.14	-2.78 ± 7.78
Glucosamine		6.86 ± 0.62	1.79 ± 1.65
Ribose		19.04 ± 4.39	2.29 ± 1.92
Gluconolactone		6.18 ± 3.15	31.35 ± 2.04
Amberlite ^c		55.83 ± 1.86	

^a All the tests were performed by shaking a suspension of 100 mg solids in 50 mL boron solution (initial concentration of boron: 300 mg L^{-1} ; pH = 9.20) at 25°C . All tests were performed in triplicate. ^b X represents the functional groups immobilized onto the surface of poly(β -CD)-*co*-(β -CD-(N₃)₇) and poly(β -CD-(N₃)₇). ^c Amberlite (IRA 743) is a commercial resin modified with *N*-methyl-D-glucamine and was used in a control experiment.

adsorption capacity of poly(β -CD)-*co*-(β -CD-(N₃)₇)@ribose ($19.04 \pm 4.39 \text{ mg g}^{-1}$), which is in accordance with the above-mentioned speculation that separated spatial configuration will not favour the formation of stable borate esters.

Finally, GNs immobilized with chain-type polyols were used for boron adsorption. The poly(β -CD)-*co*-(β -CD-(N₃)₇)@gluconolactone showed a similar sorption capacity ($6.18 \pm 3.15 \text{ mg g}^{-1}$) as the pyranose-containing polymers and only 1/3 of that of the ribose-containing GNs, which further proved that *cis*-diols of the pyranoses could coordinate with boron more efficiently and stably. To our surprise, the poly(β -CD-(N₃)₇)@gluconolactone showed an adsorption capacity of $31.35 \pm 2.04 \text{ mg g}^{-1}$, which was 5 times higher than that of poly(β -CD)-*co*-(β -CD-(N₃)₇)@gluconolactone. It is worth noting that theoretically poly(β -CD-(N₃)₇)@gluconolactone contains only ~ 2.3 times more *N*-(prop-2-yn-1-yl)*D*-gluconamide than poly(β -CD)-*co*-(β -CD-(N₃)₇)@gluconolactone, which was calculated according to the content of azide by elemental analysis. It was hypothesized that the polyols tend to have a longer and softer chain than the pyranoses or furanoses with rigid ring structures and this may also facilitate the match of *cis*-diols with boron. All these results proved that the immobilization of functional polyols could endow the glycopolymers with boron adsorption abilities.

To further prove the chemical adsorption nature of the boron removal, TGA and DSC were used to investigate the changes in the thermal degradation of the GNs before and after the adsorption of boron. As shown in Fig. 5A, the degradation of poly(β -CD)-*co*-(β -CD-(N₃)₇)@ribose started slowly after $\sim 150^\circ\text{C}$ and accelerated after $\sim 250^\circ\text{C}$, which led to a weight retention ratio of 20% at 700°C . While after boron adsorption, the degradation of the poly(β -CD)-*co*-(β -CD-(N₃)₇)@ribose-borate product only started after $\sim 240^\circ\text{C}$ and accelerated after $\sim 280^\circ\text{C}$ and finally led to a higher weight retention ratio ($\sim 25\%$) at 700°C . Further TGA characterization of poly(β -CD-(N₃)₇)@gluconolactone also revealed a higher degradation starting temperature and a higher weight retention ratio after boron adsorption. This phenomenon suggested that the coordination of *cis*-diols with boron made the GNs more stable during thermal degradation. The higher weight retention ratio could be due to the higher stability of the inorganic boron salt compared with the degradable organic polymers.

Subsequent DSC analysis, as shown in Fig. 5B, revealed the presence of large and broad exothermic peaks above 200°C , which were typical signs of side reaction such as oxidation, cross-linking or solidifying during thermal degradation. The exothermic peak temperature of poly(β -CD)-*co*-(β -CD-(N₃)₇)@ribose significantly increased from 298°C to 310°C after the adsorption of boric acid, which was in accordance with the shift of the degradation temperature in the TGA analysis. The melting temperature (T_m) for poly(β -CD)-*co*-(β -CD-(N₃)₇)@ribose, which was revealed by the endothermic peaks below 100°C , also shifted from 55°C to 65°C after boron adsorption. The T_m and degradation temperature also changed due to adsorption of boron for poly(β -CD-(N₃)₇)@gluconolactone. All of these results successfully proved the chemical coordination of boron to the *cis*-diol-containing GNs, which unavoidably changed the structures and properties of the final adsorbent-borate products.

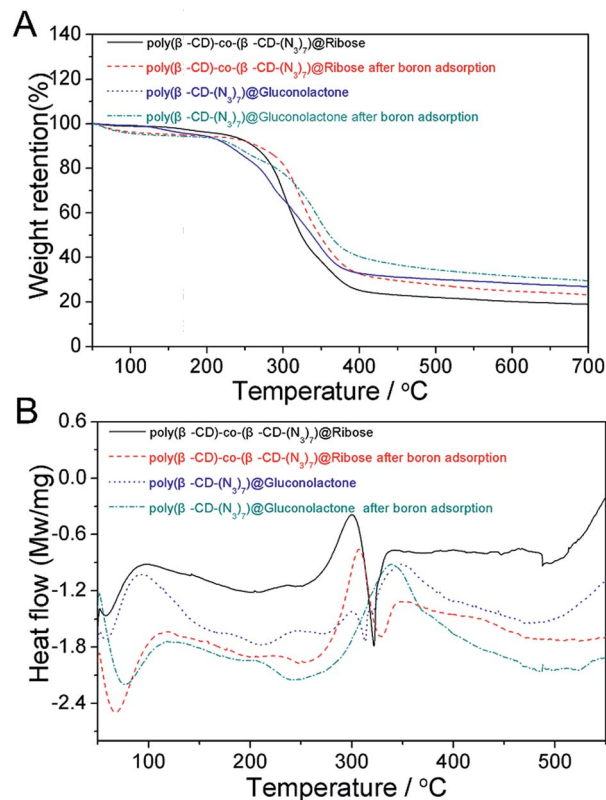


Fig. 5 TGA curves (A) and DSC scans (B) of poly(β -CD)-*co*-(β -CD-(N₃)₇)@ribose and poly(β -CD-(N₃)₇)@gluconolactone before and after the adsorption of boric acid.

Polyols have strongly pH-dependent adsorption capacities for boron since polyols react preferentially with boronate anions. The optimised pH is around 9.0–9.5, at which the dominant species is the boronate anion ($\text{B}(\text{OH})_4^-$) rather than boric acid (H_3BO_3) thus the coordination with *cis*-diols would be more efficient.^{4,59,60} The pH effect on the adsorption of boron by two typical GNs, poly(β -CD)-*co*-(β -CD-(N₃)₇)@ribose and poly(β -CD-(N₃)₇)@gluconolactone was systematically studied over a pH range from 5.0 to 11.0. As shown in Fig. 6, the Q_e of each glycopolymer adsorbent increased pronouncedly with increasing pH until pH 9.0 and subsequently decreased from pH 9.0 to 11.0. This is ascribed to the fact that $\text{B}(\text{OH})_4^-$ is the dominant species, according to the pK_a of 9.25, under slightly alkaline conditions, which favours the generation of boronate esters *via* coordination with polyols. It is worth noting that the glyco-clusters still showed considerable adsorption capacity around neutral pH, however, the adsorption capacity decreased significantly at relatively extreme pH values such as 5.0 or 11.0.

The variation of boron adsorption as a function of contact time is shown in Fig. 7 using poly(β -CD)-*co*-(β -CD-(N₃)₇)@ribose and poly(β -CD-(N₃)₇)@gluconolactone as the adsorbents. In both cases, the boron sorption is a relatively slow process and needs four hours to reach $\sim 90\%$ of the total capacity. It was interesting to find that the ribose-containing glycoclusters could reach $\sim 37\%$ of their total boron capacity in 20 min, which was faster than the glycoclusters immobilized with more chain-type polyols, which only reached $\sim 29\%$ of their total efficiency

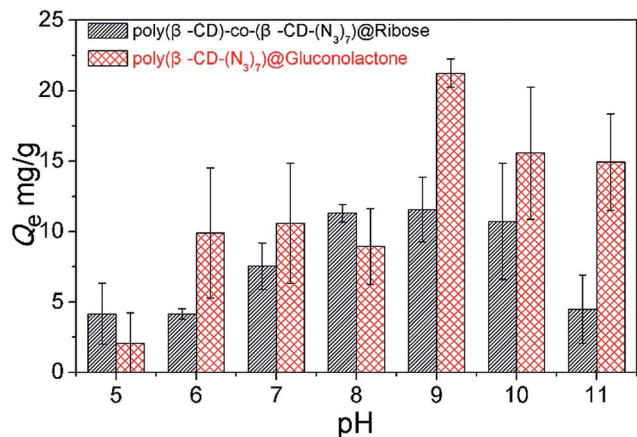


Fig. 6 Effects of pH on the boron adsorption of poly(β-CD)-co-(β-CD-(N₃)₇)@ribose and poly(β-CD-(N₃)₇)@gluconamide (100 mg GNs in 50 mL boron solution, C₀ = 300 mg L⁻¹; 25 °C).

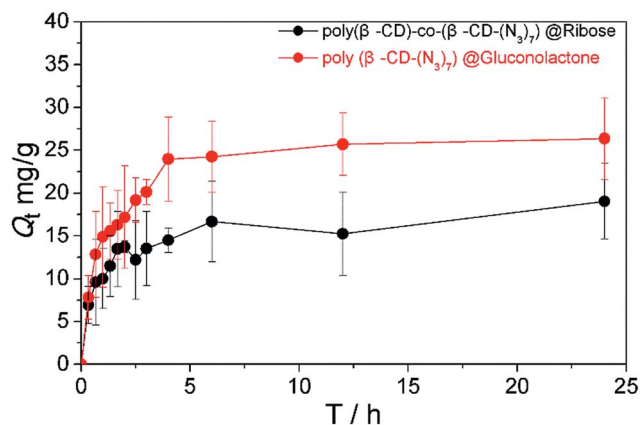


Fig. 7 Boron adsorption kinetics expressed as adsorbed concentration (Q_e, mg g⁻¹) at a given time (T, h) for different GN adsorbents (100 mg GNs in 50 mL boron solution, C₀ = 300 mg L⁻¹, pH = 9.20; 25 °C).

in 20 min. This suggests that ribose-containing glycoclusters have higher efficiency, especially in the early period of boron adsorption. Previously reported mesoporous resins or silicas containing polyols have shown faster adsorption rates with a total efficiency of up to 90% obtained in several minutes.^{60,61} TCL-cross-linked GNs in this research have shown much smaller SSAs (<20 m² g⁻¹) than previously mentioned mesoporous materials (even up to 877.7 m² g⁻¹), which may prevent the efficient contact of boron with the functional saccharides within the pores, thus resulting in a slower adsorption rate.

The kinetic data were subsequently described by pseudo-first-order and pseudo-second-order kinetics models. The pseudo-second-order kinetics model generally fits the kinetic data better (as indicated by the R² values), which justifies the adsorption mechanism with a high correlation coefficient (Table S1†) for GN adsorbents. This indicates that the exchange-adsorption rate is mainly controlled by a chemical process and thus supports the adsorption of boron *via* the formation of boronate esters.

The regeneration of GNs for boron removal was subsequently investigated. Regeneration performed by a combination of acid elution (such as 1.0 M HCl solution) and base neutralization (such as 0.1 M NaOH solution), which would destroy the borate esters and reactivate the amine groups separately, was the most frequently-used strategy in previous reports.^{8,60} In our system, no amine groups exist in the GNs and thus no base was needed for the regeneration. Thus efficient elution using acid solution and deionized water was utilized to regenerate the GNs. At first, 1.0 M HCl solution was trialled to destroy the borate ester, however, the acid was so strong that the ester type cross-linkers were also destroyed and hydrolysis of the GNs occurred. Then, milder acid solution with a pH of 3.0 was utilized for the regeneration. As shown in Fig. 8, poly(β-CD)-co-(β-CD-(N₃)₇)@ribose and poly(β-CD-(N₃)₇)@gluconolactone were utilized in five adsorption/desorption cycles. During the tests, a gradual decrease of adsorption capacity was observed and only ~20% of the pristine adsorption capacity was left over the five regeneration cycles. It was hypothesized that the regeneration was significantly affected by the pH of the elution solution and desorption may not have completely happened under such mild conditions.

In summary, the GNs have shown varied adsorption capacities for boron under different conditions, which were mainly dependant on the structure of the GNs and the immobilized polyols as well as the pH value of the solutions. The kinetic studies show that the adsorption fits a pseudo-second-order kinetic model and is mainly controlled by a chemical reaction, however, the small SSAs of the mesoporous materials resulted in a relatively slow adsorption rate. The decrease of the adsorption capacity found during the repeated adsorption/desorption tests was possibly due to the mild reaction conditions utilized. Different crosslinking reagents such as more stable tetrafluoroterephthalonitrile *etc.* or more violent regeneration conditions could be an option to improve the adsorption properties in future research.

Adsorption of methylene blue (MB) by the GNs

Cross-linked CD polymers and GNs were studied to determine the adsorption isotherms, adsorption kinetics and regeneration

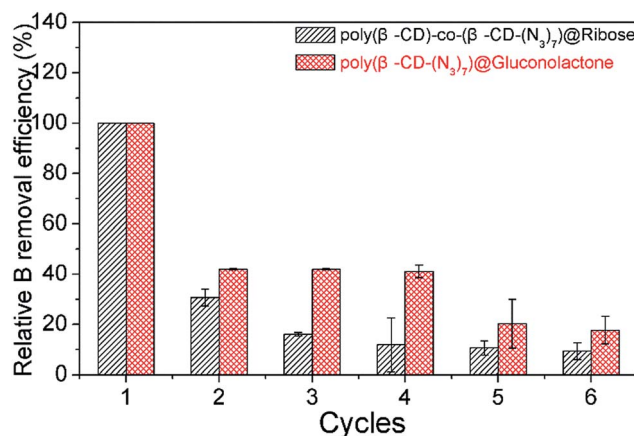


Fig. 8 Regeneration of GNs for the adsorption of boron (dose of 2 g L⁻¹; HCl acid solution, pH 3.0; equilibrium time of 12 h; 100 mg GNs in 50 mL boron solution, initial concentration of 300 mg L⁻¹; 25 °C).

using MB as a model organic pollutant. MB is a cationic dye with wide applications in the printing industry and has been studied as a typical compound for encapsulation by CD polymers. Fig. 9A compares the adsorption isotherms of MB for the different GN adsorbents, plotted as the adsorbed-phase concentration (Q_e , mg g^{-1}) vs. the aqueous-phase concentration (C_e , mg L^{-1}) at equilibrium. The adsorption data were fitted with two commonly used nonlinear adsorption models: the Freundlich model, $Q_e = K_F C_e^n$, where K_F ($\text{mg}^{1-n} \text{L}^n \text{g}^{-1}$) is the Freundlich affinity coefficient and n (unitless) is the Freundlich linearity index; and the Langmuir model, $Q_e = \frac{K_L C_e}{1 + K_L C_e} Q_{\text{max}}$, where K_L (L mg^{-1}) is the Langmuir affinity coefficient and Q_{max} (mg g^{-1}) is the maximum adsorption capacity.

The model fitting parameters are summarized in Table S2.† The Freundlich model generally fits the adsorption data better in the concentration range measured (as indicated by the R^2 values >0.95). The adsorption capacity for MB could reach an astonishing $1155 \pm 124 \text{ mg g}^{-1}$ for the poly(β -CD)-co-(β -CD-(N_3)₇), which is much higher than the most frequently-used adsorbents (activated carbon or other reported cyclodextrin-

based materials) in previous reports, which have been listed in Table S3.†^{62–66} The effects of pH or salt ion strength on the adsorption of MB by the GNs are shown in Fig. 9B. The effect of pH on the removal efficiency of MB was not significant, with only a slightly increase in alkaline solutions compared with that under acidic conditions. Addition of 0.1 M salt had no obvious influence on the MB adsorption, which indicated that the GNs showed good adsorption potential in water treatment.

The adsorption capacities (Q_e) for MB of the different GNs are listed in Table 3. Compared with poly(β -CD) which showed a capacity up to $1159 \pm 271 \text{ mg g}^{-1}$, poly(β -CD)-co-(β -CD-(N_3)₇) had a similar Q_e for MB ($1155 \pm 124 \text{ mg g}^{-1}$) under the same test conditions, while poly(β -CD-(N_3)₇) showed a much smaller Q_e ($616 \pm 112 \text{ mg g}^{-1}$). Although the slight difference in the molecular weights (MW) of β -CD and β -CD-(N_3)₇ may induce different Q_e values for the GNs, the main reason for the dramatic difference in Q_e should be attributed to the structure of poly(β -CD-(N_3)₇). Due to the totally substituted primary face of β -CD, crosslinking could only occur between the hydroxyl groups derived from the secondary face and this will unavoidably cause overlap between the bottom portals of the macrocyclic cavity as shown in Scheme 3. This may further prevent the efficient encapsulation of MB into the cavities, and thus significantly decrease the adsorption of MB. Besides, the mesoporous structure would become more clogged after immobilization with more saccharides and this may not favour the encapsulation of MB.

For the poly(β -CD)-co-(β -CD-(N_3)₇)@saccharides, the Q_e values ranged from 821 ± 21 to $1152 \pm 218 \text{ mg g}^{-1}$ (Table 3). It is worth noting that there was 0.85 mmol of azide groups per gram of poly(β -CD)-co-(β -CD-(N_3)₇) according to the nitrogen content by EA, which means that the weight content of the functional monosaccharides in the GNs could range from 14% (for ribose) to 18% (for glucosamine). Thus theoretically there should be fewer CD core cavities and a lower Q_e after the click reaction. However, for the poly(β -CD-(N_3)₇)@saccharides, the Q_e generally increased even after immobilization of the monosaccharides or polyols, ranging from 553 ± 35 to $978 \pm 90 \text{ mg g}^{-1}$. We believe this could be attributed to the secondary bond interactions between MB and the saccharides, most likely, hydrogen bonding and van der Waals forces. Considering there was 1.94 mmol of azide groups per gram of poly(β -CD-(N_3)₇), the weight content of the functional monosaccharides in the GNs could range from 27% (for ribose) to 33% (for glucosamine). With much fewer CD core cavities, poly(β -CD-(N_3)₇)@glucosamine showed a much higher Q_e ($978 \pm 90 \text{ mg g}^{-1}$, almost half as much again, Table 3) and this indicates that the secondary bonding between MB and the saccharides contributes even more for the adsorption of MB rather than the host-guest interactions. The adsorption capacity for cationic MB was generally much higher compared with that of the anionic borate. It needs to be noted that there are no other efficient ways to remove boron from water other than coordination with *cis*-diol-containing compounds. However, MB could be encapsulated into the hydrophobic cavities of the porous CD polymers. The presence of hydroxyl-rich saccharides could enhance the adsorption *via* hydrogen bonding and van der Waals forces *etc.*

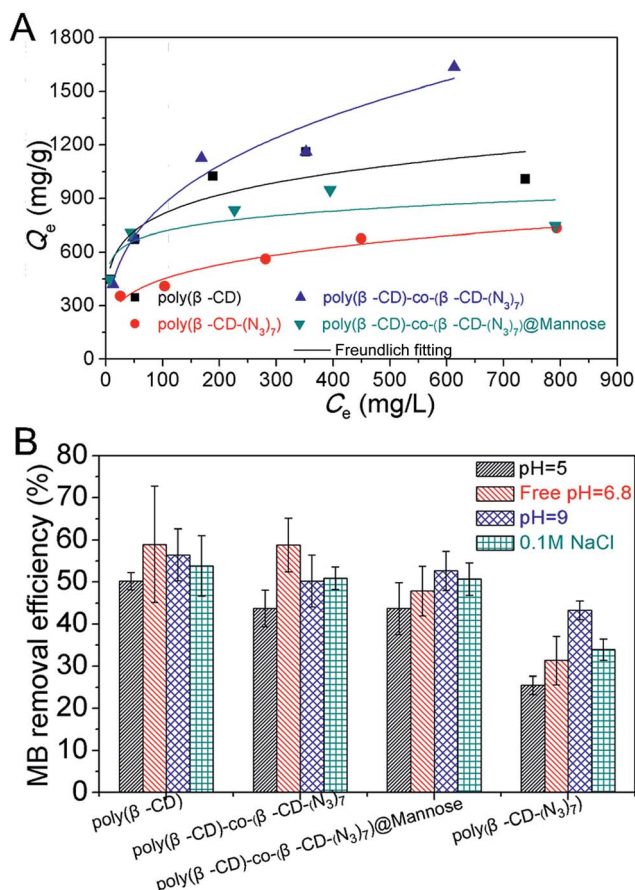
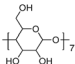
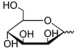
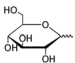
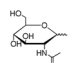
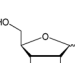
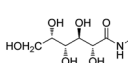
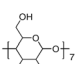
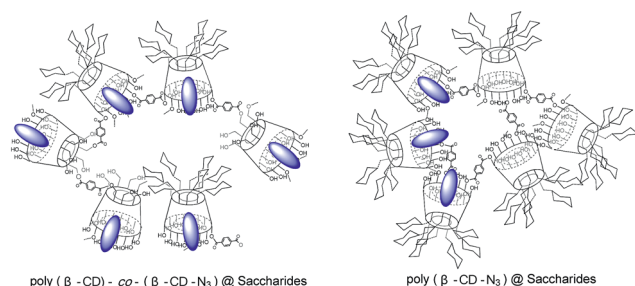


Fig. 9 Adsorption isotherms plotted as the adsorbed-phase concentration (Q_e) vs. the aqueous-phase concentration (C_e) at equilibrium for the different GN adsorbents ((A), Freundlich fitting) and the effect of pH and salt ions (B) on MB adsorption by the GNs (10 mg GNs in 50 mL MB solution, $C_0 = 400 \text{ mg L}^{-1}$; equilibrium time, 24 h; 25°C).

Table 3 Adsorption capacities for MB obtained by the GNs^a

Immobilized polyols (X) ^b	Structure	Sorption capacity (Q_e , mg g ⁻¹) for	
		Poly(β -CD)-co-(β -CD-(N ₃) ₇)@X	Poly(β -CD-(N ₃) ₇)@X
β -CD residual		1155 ± 124	616 ± 112
Mannose		941 ± 116	553 ± 35
Glucose		821 ± 21	583 ± 65
Glucosamine		1152 ± 218	978 ± 90
Ribose		862 ± 262	833 ± 90
Gluconolactone		1026 ± 153	723 ± 49
Poly(β -CD)		1159 ± 271	

^a All the tests were performed by shaking the suspension of 10 mg solids in 50 mL MB solution (initial concentration: 400 mg L⁻¹; pH = 6.8) under 25 °C. All tests were performed in triplicate. ^b X represents the functional groups immobilized onto the surface of poly(β -CD)-co-(β -CD-(N₃)₇) and poly(β -CD-(N₃)₇).



Scheme 3 Schematic representation for the encapsulation of MB by the GNs with different structures.

Compared with other adsorbents such as activated carbon, functionalized graphene oxide, β -CD-based fibres and β -CD-containing nanocomposites, which showed adsorption capacities for MB from 56.5 to 826.5 mg g⁻¹ (Table S3†), the GNs have shown more astonishing adsorption capacities as high as 1152 ± 218 mg g⁻¹. To the best of our knowledge, this is the highest adsorption capacity obtained by CD-containing polymeric adsorbents so far.

To evaluate the adsorption properties of the GNs, the MB adsorption kinetic data for different GNs are compared in Fig. 10. It can be seen that the MB adsorption rates for poly(β -CD), poly(β -CD)-co-(β -CD-(N₃)₇) and poly(β -CD-(N₃)₇) were rapid in the first 10 min, reaching ~1/3 of the adsorption capacity, followed by a long adsorption equilibrium time for the next 12 h (Fig. 10). Surprisingly, after immobilization with more saccharides the MB adsorption rates of the GNs were dramatically accelerated. It can be seen that the MB adsorption by these GNs

could reach more than 70% of the adsorption capacity within 10 min and the equilibrium time was significantly decreased to ~5 h (Fig. 10). The kinetics data of MB adsorption were also described by pseudo first-order and second-order kinetics models. As shown in Table S4†, similar to the boron kinetics data, the pseudo-second-order kinetics model generally fits the kinetic data better (the R^2 values were close to 0.99). The adsorption rate constants (k_2 , g mg⁻¹ h⁻¹, Table S4†) for the GNs were significantly higher than the values for the unmodified CD polymers, which further revealed the higher adsorption rate of the GNs. These results strongly prove that the adsorption of MB by the GNs obeys second-order adsorption kinetics and may be mainly controlled by chemical processes (hydrogen bonding *etc.*).

In order to test the regeneration of the GNs, MB adsorption was investigated over five regeneration cycles. After adsorption, the GNs were desorbed by washing first using methanol containing 5% 1 M HCl and then using DI water, and were then dried under vacuum for reuse. As shown in Fig. 11, the MB adsorption capacities of the GNs had no significant decrease over the five adsorption-regeneration cycles, which proved excellent reusability.

In summary, the GNs have demonstrated excellent adsorption rates and capacities for typical organic pollutants. Hydrogen bonding and van der Waals forces, derived from the interactions between the immobilized saccharides and MB, accelerate the adsorption rates and increase the adsorption capacities, which contribute even more than the host-guest interactions. These GNs also showed outstanding reusability during repeated adsorption/desorption cycling experiments and could potentially be used for water decontamination to remove different organic pollutants.

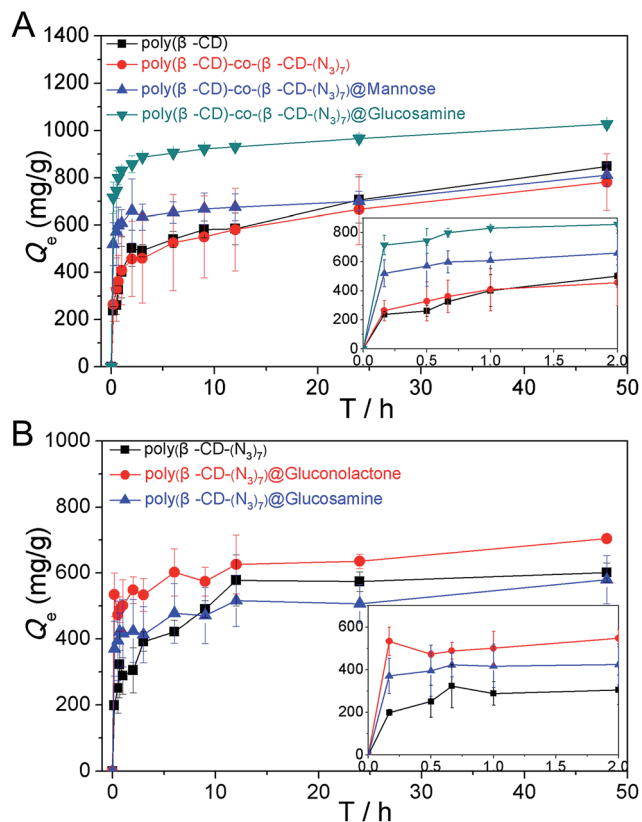


Fig. 10 Batch adsorption kinetics of MB (10 mg GNs in 50 mL MB solution, $C_0 = 400 \text{ mg L}^{-1}$, 25°C) expressed as adsorbed concentration (Q_e , mg g^{-1}) at a given time (T , h) for different GN adsorbents. Poly(β -CD) and poly(β -CD)-co-(β -CD-(N_3)₇)@saccharides (A); poly(β -CD-(N_3)₇)@saccharides (B).

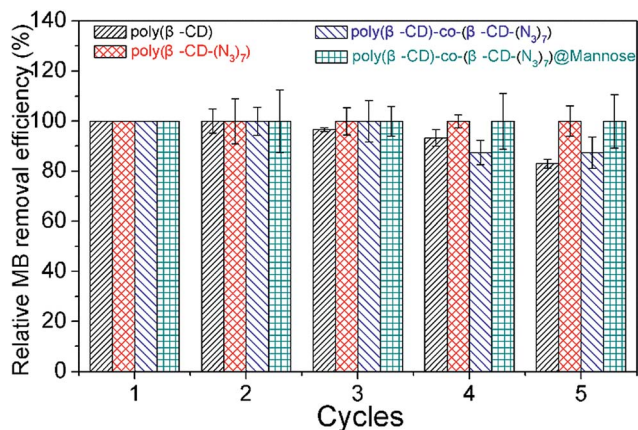


Fig. 11 Regeneration of the GNs for the adsorption of MB (dose of 0.2 g L^{-1} ; methanol containing 5% 1.0 M HCl ; equilibrium time of 24 h; 10 mg of the GNs in 50 mL MB solution, initial concentration of 400 mg L^{-1} ; 25°C).

Conclusions

In conclusion, we have successfully synthesized different functional GNs from monosaccharides and β -CD via a combination of a cross-linking reaction, Fischer glycosylation and a CuAAC click reaction. Such glycopolymers are mesoporous polymer

frameworks with multiple β -CD cores as hydrophobic cavities and persubstituted saccharides containing functional *cis*-diols on the primary face of the β -CD. The cross-linked glycopolymers have shown varied adsorption capacities for boron under different conditions, mainly affected by the structure and content of the immobilized polyols as well as the solution pH. The adsorption kinetics for boron fit a pseudo-second-order kinetic model and the adsorption is mainly controlled by a chemical reaction, however, the small SSAs of the mesoporous materials resulted in relatively slow adsorption rates. The GNs have shown excellent adsorption rates and capacities for typical pollutants using an organic dye (MB) as the adsorbate in this research. Hydrogen bonding and van der Waals forces between the immobilized saccharides and substrates significantly accelerated the adsorption rate and increased the adsorption capacity, which contributed even more than the host-guest interactions. These GNs demonstrated outstanding reusability for MB adsorption during repeated adsorption/desorption experiments, however, a decrease in the adsorption capacity for boron was observed, possibly due to the mild reaction conditions utilized.

Further optimization of the saccharide type and the spatial structure may improve the adsorption performance, stability and reusability of these materials as high-performance adsorbents. Utilization of specific cross-linking reagents such as tetrafluoroterephthalonitrile or decafluorobiphenyl *etc.* may significantly increase the SSA of the GNs as well as the adsorption performance towards micropollutants. Amine-containing polyols and saccharides such as *N*-methylglucamine *etc.* could serve as alternatives to pyranose sugars to form more stable borate esters and thus could favour the adsorption of boron. Efforts should be put into increasing the saccharide density and chain flexibility such as by using glycopolymers to replace the monosaccharides in order to increase the adsorption capacity for boron. We believe such novel bifunctional nanosponges may find potential applications in seawater desalination, boron production and water purification.

Conflicts of interest

There are no conflicts to declare.

Acknowledgements

This project was conducted with financial support from the Natural Science Foundation of China (21504044), the China Postdoctoral Science Foundation (157453) and the Natural Science Foundation of Jiangsu Province for Distinguished Young Scholars (BK20180017).

Notes and references

- 1 S. J. Kim, S. H. Ko, K. H. Kang and J. Han, *Nat. Nanotechnol.*, 2010, 5, 297.
- 2 G.-D. Kang and Y.-M. Cao, *Water Res.*, 2012, 46, 584–600.
- 3 M. A. Shannon, P. W. Bohn, M. Elimelech, J. G. Georgiadis, B. J. Mariñas and A. M. Mayes, *Nature*, 2008, 452, 301.

- 4 N. Hilal, G. J. Kim and C. Somerfield, *Desalination*, 2011, **273**, 23–35.
- 5 E. Güler, C. Kaya, N. Kabay and M. Arda, *Desalination*, 2015, **356**, 85–93.
- 6 P. H. Hermans, *Z. Anorg. Allg. Chem.*, 1925, **142**, 83–110.
- 7 J. Böeseken, in *Advances in Carbohydrate Chemistry*, ed. W. W. Pigman and M. L. Wolfrom, Academic Press, 1949, vol. 4, pp. 189–210.
- 8 H. Mishra, C. Yu, D. P. Chen, W. A. Goddard, N. F. Dalleska, M. R. Hoffmann and M. S. Diallo, *Environ. Sci. Technol.*, 2012, **46**, 8998–9004.
- 9 Y.-T. Wei, Y.-M. Zheng and J. P. Chen, *Langmuir*, 2011, **27**, 6018–6025.
- 10 J. Meng, J. Cao, R. Xu, Z. Wang and R. Sun, *J. Mater. Chem. A*, 2016, **4**, 11656–11665.
- 11 S. Morisada, T. Rin, T. Ogata, Y.-H. Kim and Y. Nakano, *Water Res.*, 2011, **45**, 4028–4034.
- 12 M. Jabli, N. Tka, K. Ramzi and T. A. Saleh, *J. Mol. Liq.*, 2018, **249**, 1138–1144.
- 13 M. Jabli, T. A. Saleh, N. Sebeia, N. Tka and R. Khiari, *Sci. Rep.*, 2017, **7**, 14448.
- 14 T. A. Saleh and I. Ali, *J. Environ. Chem. Eng.*, 2018, **6**, 5361–5368.
- 15 T. A. Saleh, I. B. Rachman and S. A. Ali, *Sci. Rep.*, 2017, **7**, 4573.
- 16 *Advanced Nanomaterials for Water Engineering, Treatment, and Hydraulics*, ed. A. S. Tawfik, IGI Global, Hershey, PA, USA, 2017.
- 17 T. A. Saleh and V. Gupta, *Nanomaterial and Polymer Membranes: Synthesis, Characterization, and Applications*, 2016.
- 18 M.-S. Steiner, A. Duerkop and O. S. Wolfbeis, *Chem. Soc. Rev.*, 2011, **40**, 4805–4839.
- 19 D. Li, Y. Chen and Z. Liu, *Chem. Soc. Rev.*, 2015, **44**, 8097–8123.
- 20 R. Ma, H. Yang, Z. Li, G. Liu, X. Sun, X. Liu, Y. An and L. Shi, *Biomacromolecules*, 2012, **13**, 3409–3417.
- 21 S. Chapelle and J.-F. Verchere, *Tetrahedron*, 1988, **44**, 4469–4482.
- 22 R. van den Berg, J. A. Peters and H. van Bekkum, *Carbohydr. Res.*, 1994, **253**, 1–12.
- 23 R. Ma and L. Shi, *Polym. Chem.*, 2014, **5**, 1503–1518.
- 24 Z. L. L. He, X. E. Yang and P. J. Stoffella, *J. Trace Elem. Med. Biol.*, 2005, **19**, 125–140.
- 25 T. Sutton, U. Baumann, J. Hayes, N. C. Collins, B. J. Shi, T. Schnurbusch, A. Hay, G. Mayo, M. Pallotta, M. Tester and P. Langridge, *Science*, 2007, **318**, 1446–1449.
- 26 A. Alsbaiee, B. J. Smith, L. Xiao, Y. Ling, D. E. Helbling and W. R. Dichtel, *Nature*, 2015, **529**, 190.
- 27 F. van de Manacker, T. Vermonden, C. F. van Nostrum and W. E. Hennink, *Biomacromolecules*, 2009, **10**, 3157–3175.
- 28 G. Crini, *Dyes Pigm.*, 2008, **77**, 415–426.
- 29 A. Z. M. Badruddoza, Z. B. Z. Shawon, W. J. D. Tay, K. Hidajat and M. S. Uddin, *Carbohydr. Polym.*, 2013, **91**, 322–332.
- 30 L. Xiao, Y. Ling, A. Alsbaiee, C. Li, D. E. Helbling and W. R. Dichtel, *J. Am. Chem. Soc.*, 2017, **139**, 7689–7692.
- 31 Y. Ling, M. J. Klemes, L. Xiao, A. Alsbaiee, W. R. Dichtel and D. E. Helbling, *Environ. Sci. Technol.*, 2017, **51**, 7590–7598.
- 32 D. M. Alzate-Sánchez, B. J. Smith, A. Alsbaiee, J. P. Hinstroza and W. R. Dichtel, *Chem. Mater.*, 2016, **28**, 8340–8346.
- 33 A. Martinez, C. Ortiz Mellet and J. M. Garcia Fernandez, *Chem. Soc. Rev.*, 2013, **42**, 4746–4773.
- 34 J. M. Benito, M. Gómez-García, C. Ortiz Mellet, I. Baussanne, J. Defaye and J. M. García Fernández, *J. Am. Chem. Soc.*, 2004, **126**, 10355–10363.
- 35 M. Gómez-García, J. M. Benito, D. Rodríguez-Lucena, J.-X. Yu, K. Chmurski, C. Ortiz Mellet, R. Gutiérrez Gallego, A. Maestre, J. Defaye and J. M. García Fernández, *J. Am. Chem. Soc.*, 2005, **127**, 7970–7971.
- 36 C. Ortiz-Mellet, J. M. Benito, J. M. G. Fernández, H. Law, K. Chmurski, J. Defaye, M. L. O'Sullivan and H. N. Caro, *Chem.-Eur. J.*, 1998, **4**, 2523–2531.
- 37 M. Massaro, S. Riela, P. Lo Meo, R. Noto, G. Cavallaro, S. Milioto and G. Lazzara, *J. Mater. Chem. B*, 2014, **2**, 7732–7738.
- 38 S. André, H. Kaltner, T. Furuike, S.-I. Nishimura and H.-J. Gabius, *Bioconjugate Chem.*, 2004, **15**, 87–98.
- 39 Y. Liu, C. Yu, H. Jin, B. Jiang, X. Zhu, Y. Zhou, Z. Lu and D. Yan, *J. Am. Chem. Soc.*, 2013, **135**, 4765–4770.
- 40 Q. Zhang, L. Su, J. Collins, G. Chen, R. Wallis, D. A. Mitchell, D. M. Haddleton and C. R. Becer, *J. Am. Chem. Soc.*, 2014, **136**, 4325–4332.
- 41 X. Shi, G. Chen, L. Yuan, Z. Tang, W. Liu, Q. Zhang, D. M. Haddleton and H. Chen, *Mater. Horiz.*, 2014, **1**, 540–545.
- 42 Y. Qu, T. Wei, W. Zhan, C. Hu, L. Cao, Q. Yu and H. Chen, *J. Mater. Chem. B*, 2017, **5**, 444–453.
- 43 W. Zhan, T. Wei, L. Cao, C. Hu, Y. Qu, Q. Yu and H. Chen, *ACS Appl. Mater. Interfaces*, 2017, **9**, 3505–3513.
- 44 H. Xiang, G. Jinbo, L. Yan, W. Ting, D. Yishi, C. Gaojian and C. Hong, *Macromol. Rapid Commun.*, 2017, **38**, 1700434.
- 45 C. Hu, J. Wu, T. Wei, W. Zhan, Y. Qu, Y. Pan, Q. Yu and H. Chen, *J. Mater. Chem. B*, 2018, **6**, 2198–2203.
- 46 W. Zhan, Y. Qu, T. Wei, C. Hu, Y. Pan, Q. Yu and H. Chen, *ACS Appl. Mater. Interfaces*, 2018, **10**, 10647–10655.
- 47 K. Chmurski and J. Defaye, *Supramol. Chem.*, 2000, **12**, 221–224.
- 48 B. Roy and B. Mukhopadhyay, *Tetrahedron Lett.*, 2007, **48**, 3783–3787.
- 49 Q. Zhang, S. Slavin, M. W. Jones, A. J. Haddleton and D. M. Haddleton, *Polym. Chem.*, 2012, **3**, 1016–1023.
- 50 M. Yurdakoç, M. Karakaplan and H. HoşGören, *Sep. Sci. Technol.*, 1999, **34**, 2615–2625.
- 51 L. D. Wilson, M. H. Mohamed and J. V. Headley, *J. Colloid Interface Sci.*, 2011, **357**, 215–222.
- 52 H. Tamai, M. Kouzu and H. Yasuda, *Carbon*, 2003, **41**, 1678–1681.
- 53 P. Lo Meo, G. Lazzara, L. Liotta, S. Riela and R. Noto, *Polym. Chem.*, 2014, **5**, 4499–4510.
- 54 J. S. Basuki, L. Esser, H. T. T. Duong, Q. Zhang, P. Wilson, M. R. Whittaker, D. M. Haddleton, C. Boyer and T. P. Davis, *Chem. Sci.*, 2014, **5**, 715–726.

- 55 C. Jie, F. Zhi-jie, W. Guang-hui, J. Yu-hua and Z. Bao-hui, *Chin. J. Synth. Chem.*, 2009, **17**, 603–605.
- 56 F. Cheng and F. Jakle, *Polym. Chem.*, 2011, **2**, 2122–2132.
- 57 A. P. Vogt, V. Trouillet, A. M. Greiner, M. Kaupp, U. Geckle, L. Barner, T. Hofe and C. Barner-Kowollik, *Macromol. Rapid Commun.*, 2012, **33**, 1108–1113.
- 58 J. Rohovec, T. Maschmeyer, S. Aime and J. A. Peters, *Chem. – Eur. J.*, 2003, **9**, 2193–2199.
- 59 R. Boncukcuoğlu, A. Erdem Yılmaz, M. Muhtar Kocakerim and M. Çopur, *Desalination*, 2004, **160**, 159–166.
- 60 N. Öztürk and T. E. Köse, *Desalination*, 2008, **227**, 233–240.
- 61 C. Sanfeliu, R. Martinez-Manez, F. Sancenon, J. Soto, V. Puchol, P. Amoros and M. D. Marcos, *J. Mater. Chem.*, 2012, **22**, 25362–25372.
- 62 F. Zhao, E. Repo, D. Yin, Y. Meng, S. Jafari and M. Sillanpää, *Environ. Sci. Technol.*, 2015, **49**, 10570–10580.
- 63 R. Zhao, Y. Wang, X. Li, B. Sun and C. Wang, *ACS Appl. Mater. Interfaces*, 2015, **7**, 26649–26657.
- 64 J. Liu, G. Liu and W. Liu, *Chem. Eng. J.*, 2014, **257**, 299–308.
- 65 X. Zhang, H. Li, M. Cao, L. Shi and C. Chen, *Sep. Sci. Technol.*, 2015, **50**, 947–957.
- 66 A. M. M. Vargas, A. L. Cazetta, M. H. Kunita, T. L. Silva and V. C. Almeida, *Chem. Eng. J.*, 2011, **168**, 722–730.